ISSN 0016-7029, Geochemistry International, 2007, Vol. 45, No. 6, pp. 590–605. © Pleiades Publishing, Ltd., 2007.
Original Russian Text © M.A. Levitan, I.A. Roshchina, A.V. Tolmacheva, 2007, published in Geokhimiya, 2007, No. 6, pp. 654–669.

Holocene History of Ob River Discharge According to Lithological and Geochemical Data

M. A. Levitan, I. A. Roshchina, and A. V. Tolmacheva

Vernadsky Institute of Geochemistry and Analytical Chemistry, Russian Academy of Sciences, ul. Kosygina 19, Moscow, 119991 Russia

e-mail: levitan@geokhi.ru

Received October 20, 2005

Abstract—Riverine water and sediment discharge to the Arctic Ocean is among the most important parameters influencing Arctic climate. It is clear that the evaluation of Arctic paleoclimate requires information on the paleodischarge of major rivers entering the sedimentation basin. Presently, the water discharge of the Ob River accounts for about 12% of the total input of river water into the Arctic Ocean. During the investigation of the Kara Sea in the framework of the Russian–German SIRRO Project, the history of Yenisei discharge received much attention in a number of publications. This paper presents the results of lithological and geochemical investigations with application to the Holocene discharge of the Ob River. Qualitative (SiO_2, Al_2O_3, K_2O, and some modules) and quantitative (sedimentation rates and absolute masses of sedimentary material) parameters were used to characterize the history of the Ob sediment discharge. It was shown that the investigated paleochannels of the Ob were initiated at the Pleistocene–Holocene boundary, and during the first half of the Holocene, the river discharge decreased irregularly with decreasing age of sediments. The observed maxima are in fairly good agreement with the data for the Yenisei. We proposed a hypothesis on the influence of glacioisostatic movements in the marginal region of the former Kara ice sheet of late Valdai age on the cessation of marine–fluvial glaciation in the paleochannels of Ob and Yenisei in the periphery of the Ob–Yenisei shoal.

DOI: 10.1134/S0016702907060079

INTRODUCTION

The investigation of Arctic climate has long established four key processes responsible for its characteristics: distribution (area) of sea ice, riverine discharge, advection of Atlantic and, in part, Pacific warm saline waters, and atmospheric Arctic variations [1]. The discharge of river water into the Arctic Ocean accounts for 10% of the global input into the ocean [2] and influences the stratification of the water body, its thermohaline circulation, biological and biochemical processes, degree of sea ice development, temperature of the near-water atmosphere, and other phenomena. Furthermore, through the mechanism of the Transpolar Drift, the transformed river waters migrate from the Arctic Ocean into the Norwegian–Greenland Basin contributing to the formation of the global salinity conveyor, which affects the circulation of the whole ocean. Because of this, the liquid discharge of Arctic rivers, which accounts for about half of freshwater input into the Arctic Ocean, has received considerable attention in the research programs of Arctic countries and in a number of international programs (e.g., APARD, SIRRO, LOIRA, Geosystem of the Laptev Sea, etc.). Sediment discharge also plays an important role; it is a significant source of sedimentary materials for the bottom deposits of Arctic seas and deep regions of the Arctic Ocean. Hydrological studies showed that there are both a strong positive correlation between the water and sediment discharges of the Arctic and a distinct seasonal character of the discharge resulting in that, on average, almost 80% of its annual amount is confined to May–June [3]. Data on river discharge is necessary for the understanding of modern Arctic climate, and to the same extent, information on paleoriver input into the Arctic Ocean is needed for the correct interpretation of the paleoclimate of Holocene geologic history. This factor is especially important in connection with the global warming of the last century and discussions on the possible role of the anthropogenic factor in this process.

Over many years, we have studied the Kara Sea, which receives the great Siberian rivers of Yenisei and Ob. We previously reported our data on the Holocene history of Yenisei discharge [4] and reviewed a number of other publications on this topic. In contrast, the Holocene history of Ob discharge has received little attention in the literature. The importance of such studies is emphasized by the fact that the liquid discharge of the Ob accounts for more than 12% of the annual river input into the Arctic Ocean [3], and in terms of the annual sediment discharge the Ob is the third largest Arctic river after the MacKenzie and Lena [3].

It should be noted that the history of river discharge can be estimated both qualitatively and quantitatively using existing age models, and geophysical data are of special importance for such reconstructions. A number of particular indicators (mineralogical, geochemical,

micropaleontological, isotopic, etc.) are used for qualitative estimates, and among quantitative parameters are the rate of sedimentation and the absolute masses of sedimentary material. However, a transition from these parameters to the values of suspended matter and water discharges is a major scientific challenge, which is not yet fully understood. Therefore, strictly speaking, our analysis is limited in fact to some semiquantitative characteristics of several aspects of the evolution of complex hydrological systems.

MATERIALS AND METHODS

The main targets of our study were two columns of bottom sediments recovered and described during the cruise of 2003 of the R/V *Akademik Boris Petrov* (BP03-07 and BP03-19). They were located north of the zone of mixing of river and sea water in the submersed river valleys of the Proto-Ob (facies zone C4 [5]) along a submeridional Ob transect, which was studied by us during cruise 49 of the R/V *Dmitrii Mendeleev* in 1993. The location of the two columns is given in Table 1 and Fig. 1. Also shown are data on col-

Table 1. Location of the columns from the Ob transect described in this paper

Column	Latitude, N	Longitude, E	Sea depth, m	Column length, cm
BP03-19	73°59.99′	73°07.81′	34	672
BP03-07	75°33.61′	73°07.64′	108	390
DM 4397	76°00.00′	72°02.30′	150	384

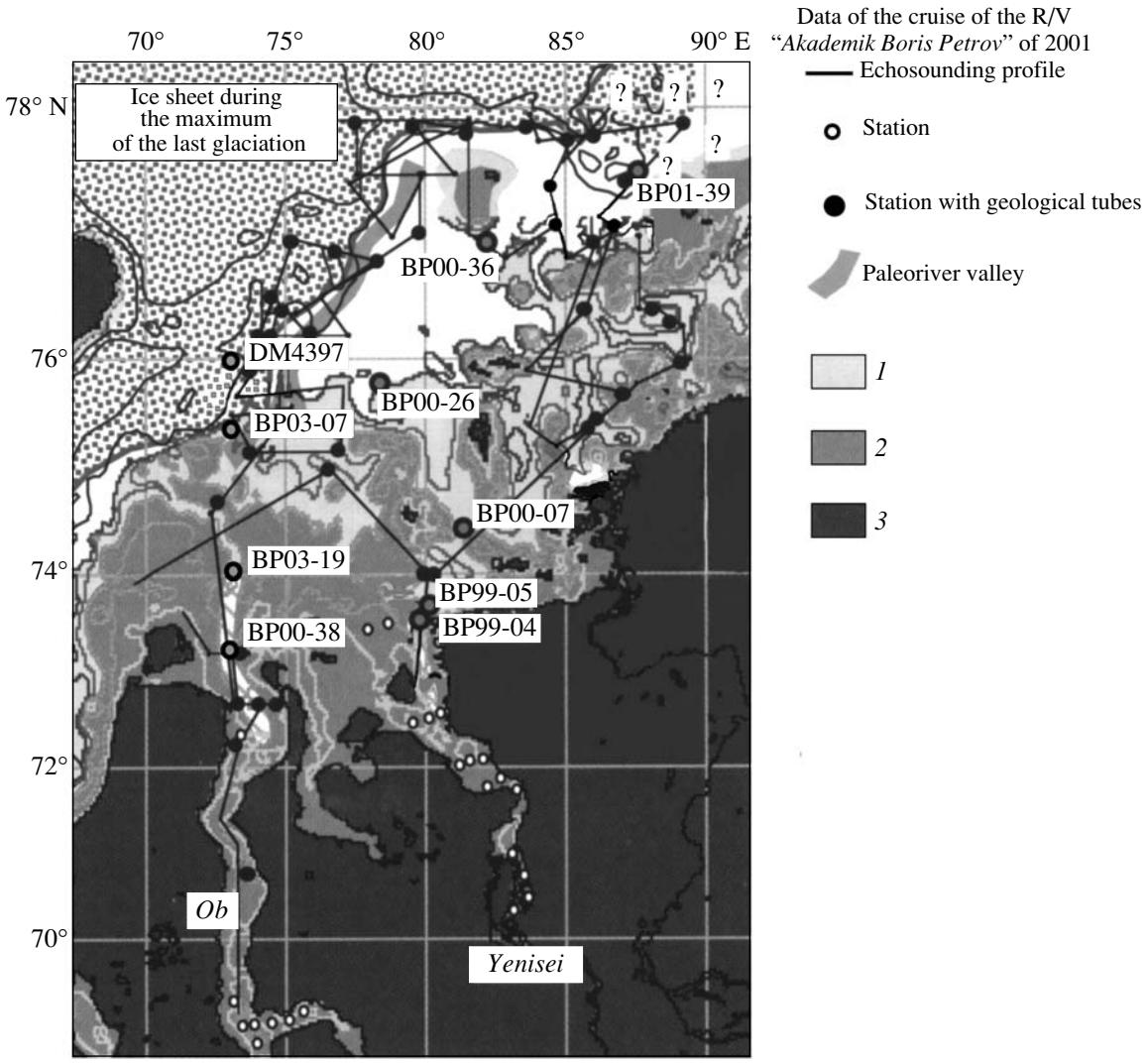

Fig. 1. Location of the columns considered in this paper in the Kara Sea after [10] modified by the authors. (*1*) Land at 11 calendar kyr BP (sea level was –50 m), (2) land at 9 calendar kyr BP (sea level was –30 m), and (3) modern land.

umn DM 4397, which is located further to the north along the same transect (facies zone D1) and was used for the comparison with the above columns, and some columns from the Yenisei transect, which will be discussed below.

The choice of sites for the coring of sediments from the R/V *Akademik Boris Petrov* was performed using a new parametric ATLAS PARASOUND III seismoacoustic profilograph, which was subjected to certification tests [6]. A sequence of finely stratified sediments was detected at both sites. Its thickness was up to 4 m at station BP03-07 and up to 9.5 m at station BP03-19.

The lithology of the bottom sediments was described by M.A. Levitan and V.V. Krupskaya [7, 8]. Their physical properties were investigated by L.N. Vlasova, and mollusk shells were identified by E.A. Frolova [7]. Granulometric, chemical, and radiocarbon analyses were carried out in onshore laboratories. Grain-size compositions were determined at the Analytical Laboratory of the Shirshov Institute of Oceanology, Russian Academy of Sciences using the method of Patelin [9] under the supervision of V.P. Kazakova. The sand–silt and silt–pelite boundaries were taken to be 0.05 and 0.005 mm, respectively.

I.A. Roshchina conducted the X-ray fluorescence analysis of bottom sediments for major oxides (complete silicate analysis) and some trace elements including S, V, Co, Ni, Zn, Rb, Sr, Y, Zr, and Ba at the Vernadsky Institute of Geochemistry and Analytical Chemistry, Russian Academy of Sciences. Measurements were carried out using a PW 1600 multichannel spectrometer (with an X-ray tube as an excitation source and an Rh anode, operating at U = 50 kV, I = 40 mA, and counting time of induced radiation of 60 s). For silicate analysis, a powdered sample was mixed with flux ($Li_2B_4O_7$) in the proportion 1 : 12 and fused at a temperature of 1050°C; the hot bead was flattened on a graphite substrate for cooling. Forty comparison samples (standard samples of rocks and soils with Russian and international certification) were measured. The parameters of diagrams and the accuracy of concentration determination were controlled by measuring eight standard samples: GM, BM, TB, PCC-1, MIV-1, SNS-1, PIM-1, and SMB. The concentrations of trace elements were determined in thin pellets, 20 mm in diameters, prepared by mixing samples with polystyrene as a binding agent. Standard samples of bottom sediments and some soil types (SGKh, SGkhM, SDO, SKR, SDPS, and other series) were also used for the construction of calibration diagrams.

The accuracy of X-ray fluorescence determination met the requirements of the Geological Survey of the Russian Federation to routine sample analysis. The relative standard deviations for the concentrations ranges observed in our samples were 1.2% for SiO_2; 3.5% for Al_2O_3; 6.2% for FeO; 10.0% for Na_2O, MgO, P_2O_5, K_2O, CaO, and TiO_2; 14.0% for Cr_2O_3; 17.0% for MnO; 25.0% for V, Ni, and Zr; and 28% for Co, Rb, Sr, and Ba, which were no higher than the permissible values.

Samples were collected each 5 cm in the upper levels of column BP03-19 and 10 cm at greater depths and within the entire section of column BP03-07. Granulometric and chemical characteristics were determined in the same specimens. Overall, 122 samples were analyzed.

Six shells of marine bivalve mollusks were analyzed at the Poznan Radiocarbon Laboratory (Poland) by accelerator mass spectrometry under the supervision of T. Goslar. The results are given in Table 2. The age of the reservoir was accepted for correction as 440 yr [10]. The ages were recalculated to a calendar scale using the method of [11].

RESULTS

The obtained results are described in the sequence from south to north.

Column BP03-19

The section is composed of two lithostratigraphic horizons.

The horizon of 0–152 cm is composed of fine pelitic mud (on average less than 10% sand and less that 15% silt), occasionally with lenses of fine-grained sand, 0.5–1.0 cm thick, and a 12-cm-thick interbed of silty–sandy clay at the base (Fig. 2). The uppermost 0.5-cm-thick layer shows a dark olive brown color, whereas very dark gray or, occasionally, dark olive gray colors are predominant in the deeper layers. Intact

Table 2. Results of the radiocarbon analysis of mollusk shells

Laboratory no.	Sample no.	Radiocarbon age, yr BP	Corrected age, yr BP	Calendar age, yr BP	Mollusk species
Poz-11062	BP03-07/248 cm	8990+/–40	8550	8985	*Yoldia hyperborea*
Poz–11063	BP03–07/44 cm	6010+/–40	5570	5925	*Macoma moesta*
Poz-11064	BP03-19/108 cm	595+/–30	155	Recent	*Macoma moesta*
Poz-11065	BP03-19/440 cm	8250+/–50	7810	8290	*Musculus niger*
Poz-12677	BP03-19/143 cm	595+/–30	155	Recent	*Portlandia arctica*
Poz-12678	BP03-19/608 cm	8560+/–50	8120	8580	*Portlandia arctica*

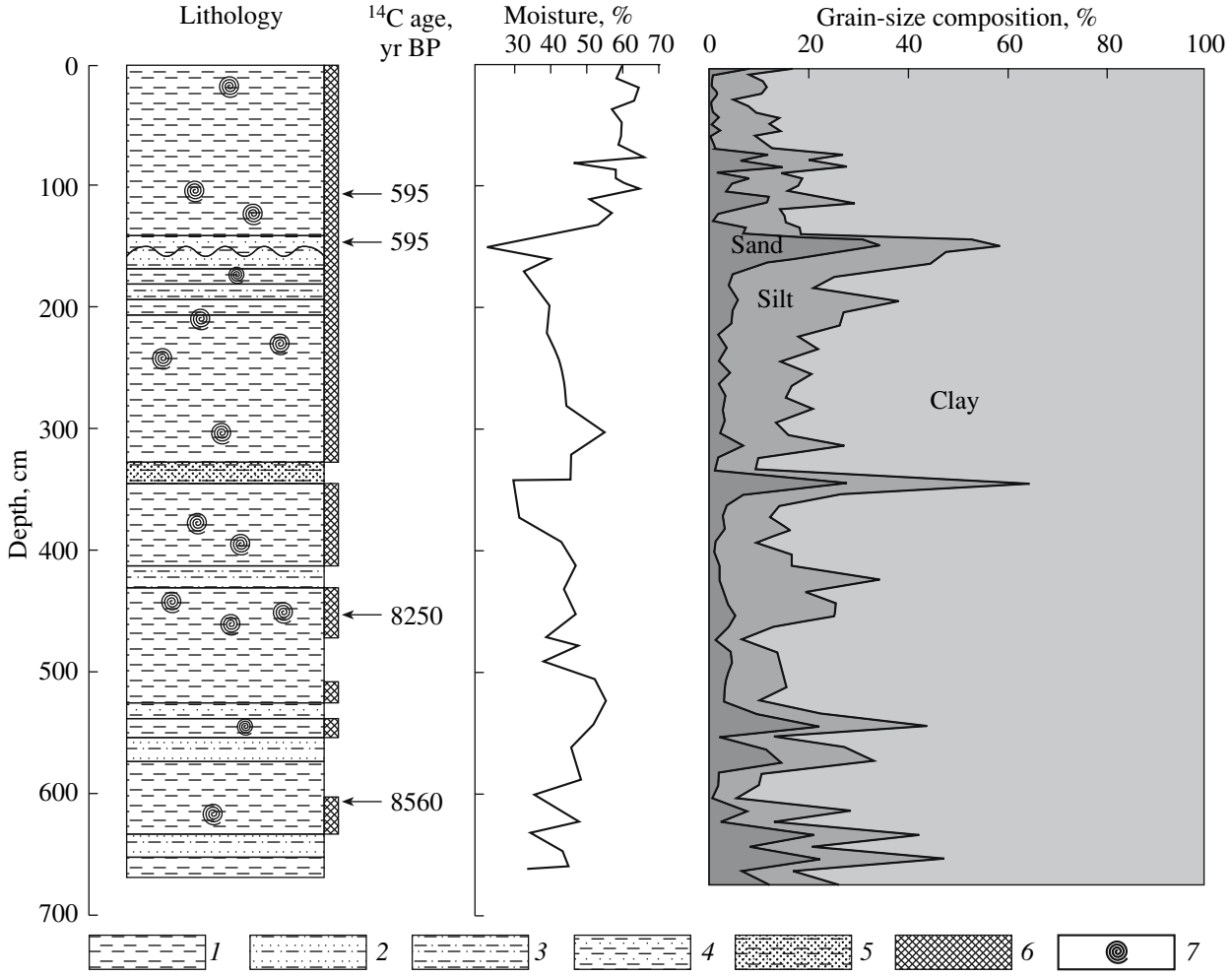

Fig. 2. Lithological characteristics, ^{14}C age, moisture content, and grain size composition of column BP03-19. (*1*) Pelitic mud, (*2*) sandy–silty clay, (*3*) silty–pelitic mud, (*4*) silty–sandy clay, (*5*) clayey–sandy aleurite, (*6*) bioturbation zone, and (*7*) mollusk shells.

shells of bivalve mollusks were encountered at levels of 10 and 108 cm. Black spots, streaks, and lenses of hydrotroilite were found below 12 cm. The accumulation of hydrotroilite sometimes imparts a black color to the sediment. Moderate bioturbation, more intense below 100 cm, was described at places. The sediments are characterized by rather high humidity and low density. The moisture content is 55–65% in the upper 100 cm and decreases abruptly at deeper levels to 22% at the boundary with the second horizon (Fig. 2). The density increases gradually from 1.28 g/cm^3 to 1.40 g/cm^3 at 125 cm and, then, increases abruptly up to 1.70 g/cm^3 [7]. Such a distribution of physical properties suggests the existence of a sedimentation gap at the boundary between this and the underlying horizon, which is represented by a weakly developed hardground.

The horizon of 152–672 cm is composed of intercalating dark gray and black pelitic muds, which dominate in the section, with subordinate layers and lenses of silty–pelitic muds and silty–sandy or sandy–silty clays of the same color (Fig. 2). The coarser units are usually no more than a few centimeters thick. The pelitic muds usually contain less than 10% sand and from 8 to 22% silt. The sediments enriched in silty and sandy fractions contain 11–34% sand and 18–33% silt (Fig. 2). Bivalve shells occur throughout the entire section; the level of 605–608 cm hosts an extensive accumulation of *Portlandia arctica* with detritus and the shells of the gastropod *Criptonatica* sp. The most extensive bioturbation and diagenetic mottling resulting from the development of hydrotroilite aggregates were described in the interval between 150 and 385 cm. The lower part of the horizon (below 343 cm) displays the development of a distinct finely layered structure composed of intercalated lithological varieties with different shades of gray and black colors, massive or bioturbated structures, and finer or coarse textures. On average, the moisture content varies around 40% (from 30% in the coarsest sediments to 50% in the finest pelitic muds) (Fig. 2), and the density is about 1.60 g/cm^3 (from 2.00 g/cm^3 in layers enriched in silty and sandy fractions to 1.40 g/cm^3 in pelitic muds).

As could be expected, the **chemical compositions** of the two horizons are strongly different. The upper horizon is enriched in Na, Mn, Al, Fe, P, and Ba but depleted in Si, Ca, Ti, S, Rb, Sr, and Zr compared with the lower horizon (Fig. 3). In general, the chemical composition of the upper horizon resembles the composition of modern facies C4 (filling the channels of an ancient river network) [5]. The lower horizon shows a complex entanglement of features observed in the modern facies of rivers (Na, Cr, Mn, Fe, V, Co, and Ni) and mixing zones (P, to some extent, Si, Al, and Ba). The correlation analysis of various oxides, elements, and grain-size fraction (Tables 3, 4) allowed us to distinguish the following associations in the upper horizon at a confidence level of 95%: (1) Na_2O and S confined to the fraction 0.50–0.25 mm (i.e., sulfide sulfur and sodium from plagioclases are predominant); (2) MgO, Al_2O_3, P_2O_5, K_2O, TiO_2, Cr_2O_3, MnO, FeO, V, and, to some extent, Ni confined to the subcolloidal fraction; and (3) SiO_2, CaO, Rb, Sr, and Ba confined to the sand and 0.05–0.01 mm fractions. These correlations are somewhat disturbed in the lower horizon, where the following associations are observed: (1) Na_2O, K_2O, Ni, and Ba confined to sands; (2) MgO, Al_2O_3, TiO_2, MnO, FeO, P_2O_5, S, and V confined to the subcolloid fraction; (3) SiO_2, CaO, Rb, Sr, Zr, and Ba confined to sands and silts (Sr significantly substitutes for Ca in large fragments of mollusk shells); and (4) Cr_2O_3 confined to the fraction smaller than 0.001 mm.

The available radiocarbon age determinations (Table 2) show that the first horizon was most likely formed relatively recently as a result of a submarine landslide. The sedimentation rate between 440 and 608 cm was 569 cm/kyr, which is within the range of modern sedimentation rates in the depocenters of the zones of mixing between river and sea waters in the southern Kara Sea [5]. The average absolute mass accumulation rates of sediments in the second horizon are 546 g/cm^2/kyr. The extrapolation of the sedimentation rate yields an age of 7.79 ka for the upper boundary of the second layer, 8.69 ka for the base of the horizon, and 9.18 ka for the sedimentary filling of the channel (the thickness of filling was estimated using the PARASOUND as 9.5 m). Taking into account that there was a certain time lag between the beginning of channel incision by river currents and the beginning of its sedimentary filling, the incipient formation of the river valley (channel) can be dated between 11 and 10 ka.

The investigation of smear slides revealed that the sediments are almost free of remains of siliceous organisms and, consequently, of biogenic opal [7]. We demonstrated previously [12] that the Ob is a potent source of quartz and potassium feldspar in the sediments of the Kara Sea. It is reasonable to suppose that the SiO_2/Al_2O_3 ratio and quartz content calculated after Gurvich [12] as $SiO_2 - 2.55\ Al_2O_3$ are indicators of the sediment discharge of the Ob. The K_2O/Al_2O_3 ratio plays the same role for potassium feldspars. Note that according to the data of German researchers [13], the K/Al and Rb/Al ratios are efficient indicators of the sediment discharge of the Ob [13], which is supported by our results. Figure 4 shows the distribution of quartz content and K_2O/Al_2O_3 in the second horizon with the age in the column. It can be seen that this ratio increases downward in the section, which can be attributed to an increase in the fraction of riverine sedimentary material. This trend includes several periods of the highest sedimentary input by the Ob River at 7.85, 8.12, 8.42, 8.5, 8.58, 8.62, and 8.68 calendar kyr.

Column BP03-07

In terms of **lithostratigraphy**, the sediments of this column belong to a single horizon. They are represented by intercalated sandy–silty and silty–sandy clays with rare thin lenses and interbeds of silty sand (with sand and silt contents of about 30 and 20%, respectively). The content of pelitic fraction usually ranges within 40–60%, occasionally higher (Fig. 5). The uppermost centimeter is made up of dark brown sediments, whereas the section is dominated by olive gray and dark olive gray colors. Polychaetes occur in the upper 30 cm. The detritus of mollusk shells (bivalves and, occasionally, gastropods) occurs over the entire section (up to 390 cm), whereas intact shells are more rare. It is interesting that the shells of *Yoldia hyperborean*, which reside now in the upper sublittoral zone no deeper than 20 m, were described in the column starting (from top to bottom) from 200 cm and down to the base of the section [7]. The development of hydrotroilite and relatively strong bioturbation occur to a depth of 85 cm and were never observed below this level. A hydrogen sulfide odor was noted from 150 cm downward in the section. Within the interval 175–320 cm, single crystals and aggregates (up to 10 cm long) of ikaite of brown and honey yellow colors were detected at levels of 175, 191, 199, 260–270, 280–285, 300–305, 315, and 320 cm. It should be noted that this is the first finding in the Ob transect. Ikaite was repeatedly described along the Yenisei transect [14–16]. In general, the number of interbeds of coarser grained varieties increases downward in the section.

The **most major elements** (Na, Mg, Al, Si, P, Ti, Fe, and Co) in the sediments correspond to those of modern river deposits and bear some resemblance to the proximal subfacies of the mixing zone [5]. A number of elements (K, Mn, Fe, Zr, and Ba) show a more complex distribution. The concentrations of S and Sr are unexpectedly high, whereas those of Ni and Rb are very low. Correlation analysis (Table 5) revealed in principle the same element associations as in column BP03-19. The following associations can be reliably distinguished: (1) MgO, Al_2O_3, K_2O, TiO_2, FeO, MnO, V, and Ni confined to two grain-size fractions, 0.005–0.001 mm and (for Fe) sandy–silty one; (2) SiO_2, Sr, Zr, Ba, and Rb confined to the 0.1–0.05 mm fraction; (3) P_2O_5 associating in part with TiO_2 and MnO; and (4) CaO, Cr_2O_3,

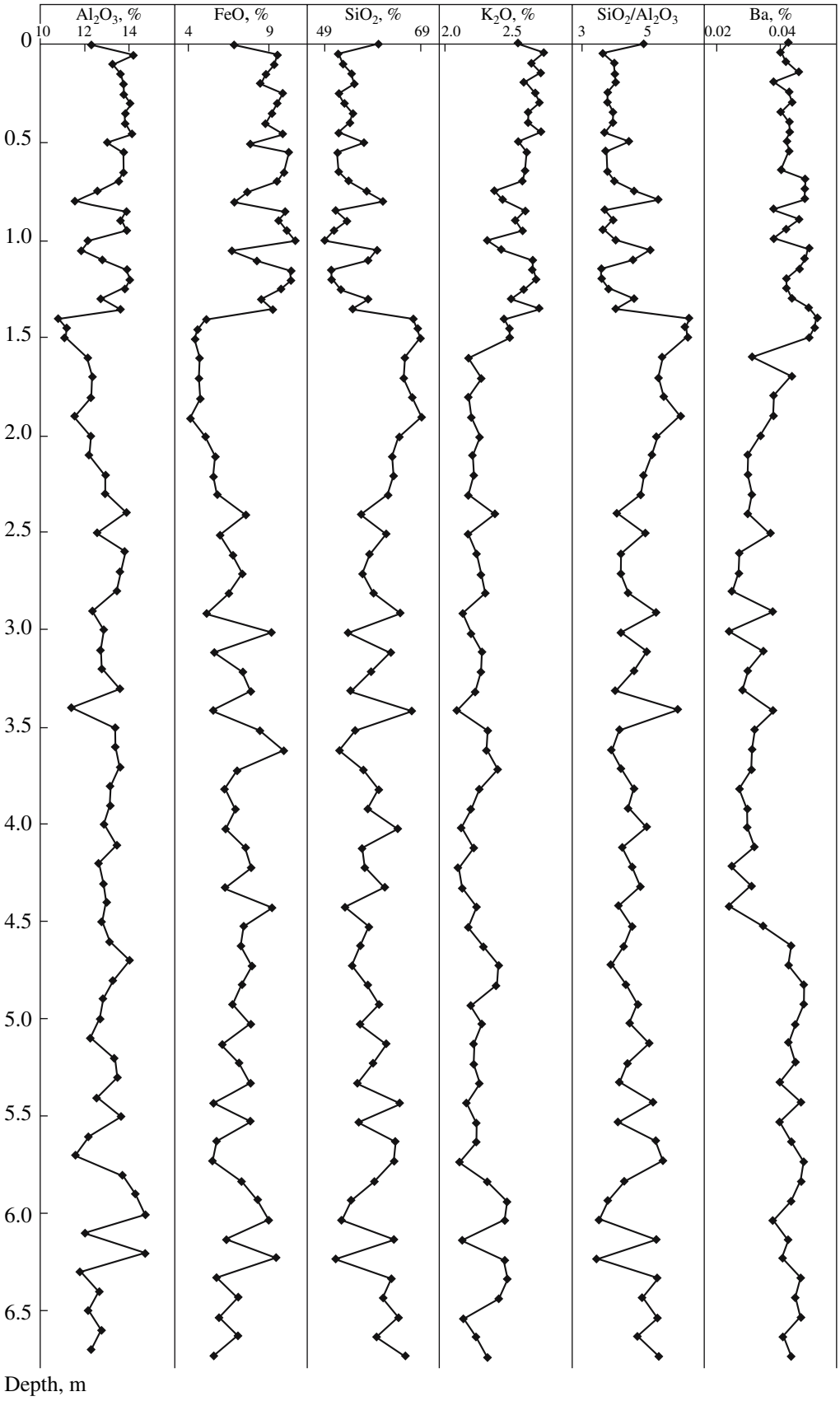

Fig. 3. Chemical composition of sediments from column BP03-19.

Table 3. Correlation matrix for column BP03-19, horizon I (n = 30)

Component	Na_2O	MgO	Al_2O_3	SiO_2	P_2O_5	K_2O	CaO	TiO_2	Cr_2O_3	MnO	FeO	S	V	Ni	Rb
Na_2O	1.00	–0.02	–0.17	–0.33	–0.51	–0.21	0.02	–0.16	–0.01	–0.04	0.18	0.65	–0.10	–0.16	–0.30
MgO	–0.02	1.00	0.87	–0.87	0.32	0.66	–0.67	0.54	0.47	0.37	0.88	0.01	0.89	0.19	–0.32
Al_2O_3	–0.17	0.87	1.00	–0.71	0.37	0.78	–0.71	0.74	0.53	0.35	0.72	–0.24	0.84	0.31	–0.07
SiO_2	–0.33	–0.87	–0.71	1.00	–0.21	–0.37	0.63	–0.39	–0.44	–0.40	–0.97	–0.40	–0.80	0.03	0.60
P_2O_5	–0.51	0.32	0.37	–0.21	1.00	0.17	–0.23	0.08	0.12	0.58	0.35	–0.40	0.50	–0.07	–0.33
K_2O	–0.21	0.66	0.78	–0.37	0.17	1.00	–0.57	0.58	0.46	0.07	0.39	–0.43	0.53	0.52	0.26
CaO	0.02	–0.67	–0.71	0.63	–0.23	–0.57	1.00	–0.40	–0.47	0.02	–0.68	0.01	–0.66	–0.44	0.11
TiO_2	–0.16	0.54	0.74	–0.39	0.08	0.58	–0.40	1.00	0.59	0.34	0.33	–0.28	0.55	0.46	0.20
Cr_2O_3	–0.01	0.47	0.53	–0.44	0.12	0.46	–0.47	0.59	1.00	0.24	0.44	–0.02	0.45	0.13	–0.01
MnO	–0.04	0.37	0.35	–0.40	0.58	0.07	0.02	0.34	0.24	1.00	0.40	–0.01	0.48	–0.26	–0.50
FeO	0.18	0.88	0.72	–0.97	0.35	0.39	–0.68	0.33	0.44	0.40	1.00	0.35	0.84	–0.04	–0.64
S	0.65	0.01	–0.24	–0.40	–0.40	–0.43	0.01	–0.28	–0.02	–0.01	0.35	1.00	–0.06	–0.45	–0.63
V	–0.10	0.89	0.84	–0.80	0.50	0.53	–0.66	0.55	0.45	0.48	0.84	–0.06	1.00	0.21	–0.37
Ni	–0.16	0.19	0.31	0.03	–0.07	0.52	–0.44	0.46	0.13	–0.26	–0.04	–0.45	0.21	1.00	0.43
Rb	–0.30	–0.32	–0.07	0.60	–0.33	0.26	0.11	0.20	–0.01	–0.50	–0.64	–0.63	–0.37	0.43	1.00
Sr	–0.19	–0.88	–0.79	0.94	–0.25	–0.53	0.81	–0.43	–0.50	–0.29	–0.96	–0.30	–0.82	–0.11	0.48
Zr	–0.18	–0.88	–0.75	0.94	–0.27	–0.45	0.62	–0.36	–0.40	–0.37	–0.96	–0.30	–0.81	0.01	0.55
Ba	–0.32	–0.37	–0.37	0.54	0.10	–0.09	0.17	–0.37	–0.14	–0.38	–0.44	–0.39	–0.17	0.19	0.31

Component	Sr	Zr	Ba	1–0.5	0.5–0.25	0.25–0.1	0.1–0.05	Sand	0.05–0.01	0.01–0.005	Silt	0.005–0.001	<0.001	Clay
Na_2O	–0.19	–0.18	–0.32	–0.09	0.55	–0.22	–0.18	–0.18	–0.15	0.09	0.06	–0.28	0.27	0.16
MgO	–0.88	–0.88	–0.37	–0.47	–0.14	–0.29	–0.73	–0.62	–0.63	–0.16	–0.23	–0.20	0.59	0.52
Al_2O_3	–0.79	–0.75	–0.37	–0.61	–0.43	–0.32	–0.76	–0.68	–0.69	–0.18	–0.26	0.07	0.48	0.52
SiO_2	0.94	0.94	0.54	0.52	–0.29	0.35	0.75	0.65	0.62	0.09	0.18	0.36	–0.66	–0.53
P_2O_5	–0.25	–0.27	0.10	–0.10	–0.33	0.13	–0.09	–0.01	0.02	0.27	0.26	–0.02	–0.03	–0.04
K_2O	–0.53	–0.45	–0.09	–0.38	–0.59	–0.18	–0.56	–0.48	–0.46	–0.25	–0.30	0.23	0.30	0.41
CaO	0.81	0.62	0.17	0.79	0.20	0.20	0.64	0.52	0.56	0.21	0.28	0.03	–0.59	–0.59
TiO_2	–0.43	–0.36	–0.37	–0.53	–0.41	–0.52	–0.69	–0.71	–0.70	–0.37	–0.45	0.32	0.15	0.29
Cr_2O_3	–0.50	–0.40	–0.14	–0.43	–0.09	–0.23	–0.53	–0.45	–0.46	–0.48	–0.51	–0.15	0.35	0.30
MnO	–0.29	–0.37	–0.38	–0.19	0.01	–0.23	–0.37	–0.33	–0.15	0.32	0.27	–0.20	–0.14	–0.23
FeO	–0.96	–0.96	–0.44	–0.52	0.25	–0.23	–0.69	–0.55	–0.54	–0.03	–0.11	–0.39	0.63	0.48
S	–0.30	–0.30	–0.39	–0.12	0.95	–0.11	–0.14	–0.10	–0.04	0.08	0.07	–0.40	0.25	0.09
V	–0.82	–0.81	–0.17	–0.52	–0.16	–0.18	–0.60	–0.49	–0.53	0.06	–0.02	–0.16	0.39	0.33
Ni	–0.11	0.01	0.19	–0.32	–0.54	–0.26	–0.34	–0.35	–0.33	–0.21	–0.24	0.38	0.12	0.29
Rb	0.48	0.55	0.31	0.19	–0.63	–0.02	0.27	0.15	–0.01	–0.29	–0.27	0.53	–0.27	–0.06
Sr	1.00	0.93	0.45	0.67	–0.18	0.26	0.76	0.63	0.61	0.11	0.19	0.25	–0.66	–0.58
Zr	0.93	1.00	0.51	0.45	–0.16	0.28	0.72	0.61	0.62	0.05	0.13	0.30	–0.67	–0.56
Ba	0.45	0.51	1.00	0.36	–0.25	0.65	0.68	0.73	0.57	0.19	0.26	0.02	–0.41	–0.41

Table 4. Correlation matrix for column BP03-19, horizon II (n = 52)

Component	Na_2O	MgO	Al_2O_3	SiO_2	P_2O_5	K_2O	CaO	TiO_2	Cr_2O_3	MnO	FeO	S	V	Ni	Rb
Na_2O	1.00	–0.47	–0.42	0.30	0.10	0.62	–0.13	–0.51	–0.21	0.11	–0.27	–0.41	0.24	0.50	–0.19
MgO	–0.47	1.00	0.89	–0.91	0.29	0.14	–0.29	0.45	0.18	0.36	0.83	0.42	0.39	–0.03	–0.10
Al_2O_3	–0.42	0.89	1.00	–0.85	0.39	0.23	–0.34	0.61	0.06	0.56	0.77	0.24	0.54	0.13	–0.26
SiO_2	0.30	–0.91	–0.85	1.00	–0.45	–0.23	0.32	–0.34	–0.16	–0.54	–0.96	–0.31	–0.55	0.03	0.37
P_2O_5	0.10	0.29	0.39	–0.45	1.00	0.13	–0.25	0.19	0.23	0.80	0.53	–0.19	0.73	0.24	–0.73
K_2O	0.62	0.14	0.23	–0.23	0.13	1.00	–0.38	–0.14	–0.16	0.37	0.21	–0.11	0.46	0.48	–0.07
CaO	–0.13	–0.29	–0.34	0.32	–0.25	–0.38	1.00	–0.04	0.06	–0.28	–0.37	0.03	–0.34	–0.18	0.08
TiO_2	–0.51	0.45	0.61	–0.34	0.19	–0.14	–0.04	1.00	0.00	0.30	0.27	0.07	0.21	0.11	–0.11
Cr_2O_3	–0.21	0.18	0.06	–0.16	0.23	–0.16	0.06	0.00	1.00	–0.02	0.22	0.26	0.12	–0.21	0.03
MnO	0.11	0.36	0.56	–0.54	0.80	0.37	–0.28	0.30	–0.02	1.00	0.59	–0.22	0.74	0.17	–0.70
FeO	–0.27	0.83	0.77	–0.96	0.53	0.21	–0.37	0.27	0.22	0.59	1.00	0.26	0.58	–0.10	–0.47
S	–0.41	0.42	0.24	–0.31	–0.19	–0.11	0.03	0.07	0.26	–0.22	0.26	1.00	–0.21	–0.36	0.35
V	0.24	0.39	0.54	–0.55	0.73	0.46	–0.34	0.21	0.12	0.74	0.58	–0.21	1.00	0.44	–0.62
Ni	0.50	–0.03	0.13	0.03	0.24	0.48	–0.18	0.11	–0.21	0.17	–0.10	–0.36	0.44	1.00	–0.16
Rb	–0.19	–0.10	–0.26	0.37	–0.73	–0.07	0.08	–0.11	0.03	–0.70	–0.47	0.35	–0.62	–0.16	1.00
Sr	0.24	–0.79	–0.68	0.83	–0.24	–0.28	0.59	–0.16	–0.19	–0.33	–0.85	–0.33	–0.37	0.16	0.09
Zr	0.30	–0.84	–0.74	0.90	–0.40	–0.22	0.42	–0.11	–0.27	–0.43	–0.90	–0.33	–0.47	0.09	0.26

Component	Sr	Zr	Ba	1–0.5	0.5–0.25	0.25–0.1	0.1–0.05	Sand	0.05–0.01	0.01–0.005	Silt	0.005–0.001	<0.001	Clay
Na_2O	0.24	0.30	0.70	0.09	–0.04	0.76	0.56	0.68	–0.26	0.26	0.05	–0.44	–0.29	–0.44
MgO	–0.79	–0.84	–0.54	–0.05	0.19	–0.58	–0.66	–0.69	–0.38	–0.57	–0.58	0.06	0.70	0.73
Al_2O_3	–0.68	–0.74	–0.35	–0.10	0.01	–0.61	–0.67	–0.71	–0.39	–0.69	–0.67	–0.03	0.79	0.79
SiO_2	0.83	0.90	0.38	0.02	–0.16	0.48	0.60	0.61	0.43	0.56	0.60	0.05	–0.70	–0.69
P_2O_5	–0.24	–0.40	0.39	0.27	–0.13	–0.16	–0.10	–0.12	–0.36	–0.30	–0.38	–0.29	0.36	0.27
K_2O	–0.28	–0.22	0.34	–0.09	0.07	0.35	0.11	0.19	–0.44	–0.20	–0.35	–0.32	0.18	0.07
CaO	0.59	0.42	0.10	0.08	–0.06	–0.02	0.12	0.08	0.15	0.13	0.17	0.17	–0.20	–0.15
TiO_2	–0.16	–0.11	–0.24	–0.04	–0.08	–0.66	–0.44	–0.55	–0.06	–0.51	–0.39	0.18	0.47	0.54
Cr_2O_3	–0.19	–0.27	–0.07	0.09	0.14	–0.21	0.14	0.05	0.00	0.11	0.08	0.04	–0.08	–0.07
MnO	–0.33	–0.43	0.32	0.10	–0.19	–0.18	–0.18	–0.20	–0.41	–0.41	–0.49	–0.18	0.43	0.38
FeO	–0.85	–0.90	–0.30	–0.03	0.14	–0.41	–0.49	–0.50	–0.44	–0.46	–0.53	–0.01	0.59	0.59
S	–0.33	–0.33	–0.55	–0.05	0.29	–0.36	–0.29	–0.33	–0.03	–0.17	–0.14	0.21	0.20	0.28
V	–0.37	–0.47	0.43	0.08	–0.10	–0.06	–0.14	–0.12	–0.52	–0.46	–0.57	–0.35	0.49	0.38
Ni	0.16	0.09	0.51	–0.03	–0.15	0.16	0.05	0.08	–0.32	–0.31	–0.37	–0.49	0.31	0.14
Rb	0.09	0.26	–0.44	–0.07	0.11	0.02	0.08	0.07	0.31	0.24	0.32	0.26	–0.29	–0.21
Sr	1.00	0.87	0.51	0.12	–0.21	0.26	0.42	0.41	0.35	0.31	0.38	–0.07	–0.43	–0.46
Zr	0.87	1.00	0.41	0.05	–0.16	0.37	0.54	0.53	0.32	0.44	0.46	0.06	–0.59	–0.57
Ba	0.51	0.41	1.00	0.10	–0.26	0.52	0.51	0.55	–0.24	0.07	–0.06	–0.45	–0.15	–0.31

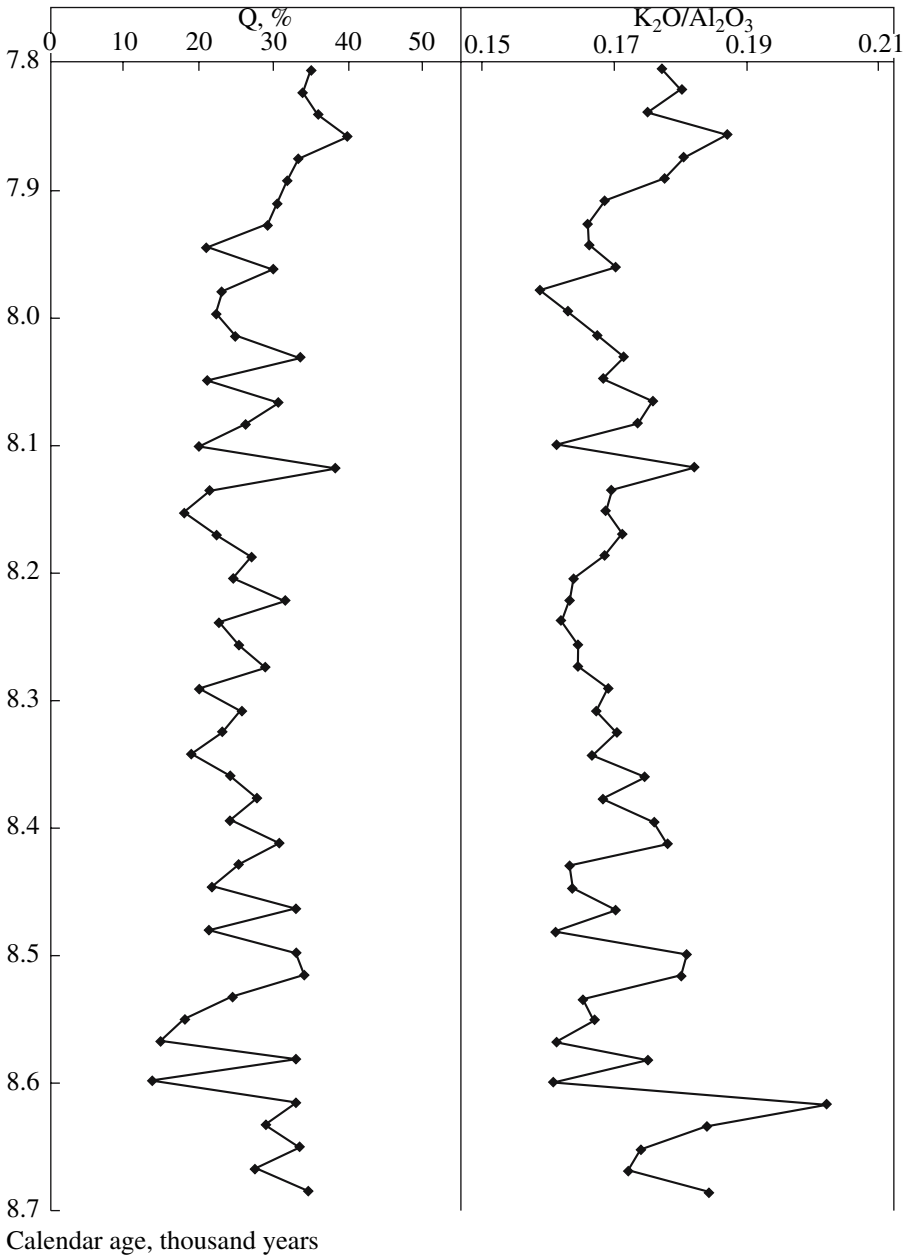

Fig. 4. Distribution of indicator parameters of the sediment discharge of the Ob River, quartz content (Q) and K_2O/Al_2O_3 ratio, against the age of sediments in the second horizon of column BP03-19.

and S showing no associations with other elements; sulfur is definitely confined to the subcolloidal fraction.

In agreement with the distribution of lithological compositions, the concentrations of most elements correlated with sandy–silty fractions (for instance, SiO_2 and Ba) and SiO_2/Al_2O_3 indicator ratio increase from top to bottom in the section (Fig. 6); this trend begins to be observable from different depths for different elements (for instance, from 125 cm for Si, 115 cm for Sr, and 305 cm for Zr). The enrichment of sulfur downward in the section is probably related to the same behavior of C_{org}.

The available radiocarbon age determinations allowed us to calculate the average sedimentation rate as 67 cm/kyr. The average absolute mass accumulation rates of sedimentary material are 94 g/cm^2 /kyr. An age of 5.27 calendar kyr was obtained for the roof of the section, 11.1 calendar kyr for the base of the column, and 11.25 calendar kyr for the sedimentary filling of the channel. Thus, the ages of the generation of Proto-Ob channels are approximately equal at the two stations and correspond to the beginning of the Holocene.

An irregular increase in the bulk content of quartz with increasing sediment age is clearly seen in Fig. 7.

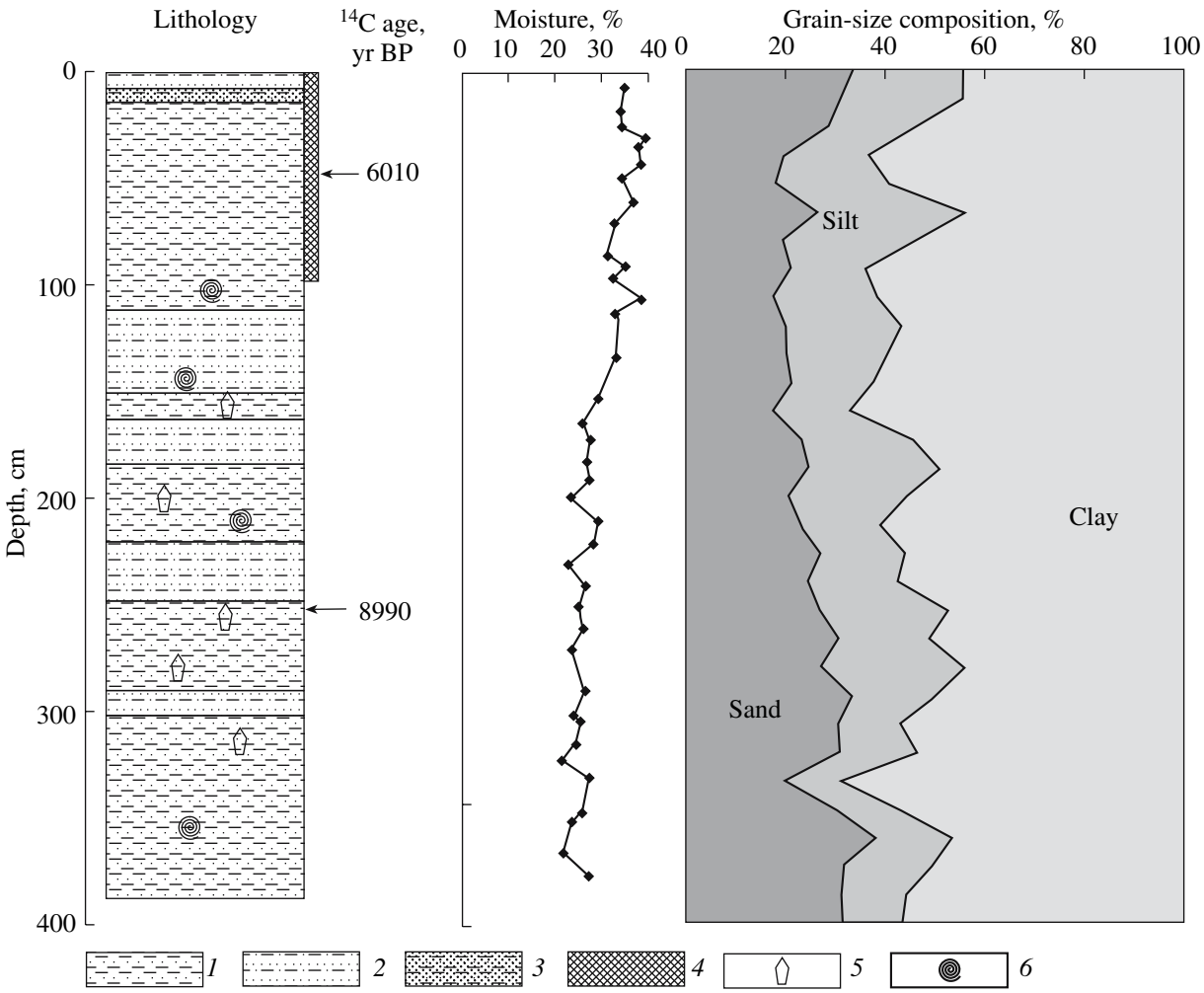

Fig. 5. Lithological characteristics, ^{14}C age, moisture content, and grain-size composition of column BP03-07. (*1*) Silty–sandy clay, (*2*) sandy–silty clay, (*3*) clayey–sandy aleurite, (*4*) bioturbation zone, (*5*) ikaite, and (*6*) mollusk shells.

The peaks of K_2O/Al_2O_3 practically coincide with quartz peaks, although the trend of increase in this ratio downward in the section is much less pronounced than that for quartz.

Based on the K_2O/Al_2O_3 values and quartz contents, the following periods of the maximum sediment discharge of the Ob can be distinguished: 6.5, 7.2, 8.3, 9.6, 9.8–10.0, and 10.3–10.7 calendar kyr (Fig. 7). Recall that only the lower part of the Holocene was exposed in the section. Note that the first two maxima correspond to the periods of elevated Yenisei discharge at 7.5–6.2 calendar kyr, whereas those older than 7.9 and, especially, older than 9.4 calendar kyr correspond to its maximum sediment discharge [5].

The maxima of river discharge recorded in columns BP03-07 and BP03-19 should be compared taking into account the significantly higher sedimentation rates in the latter column and, correspondingly, much higher time resolution between samples. In such a case, the time between neighboring maxima of sediment discharge may be from several tens to several hundreds of years. Taking into account the density of sampling and lithological description, especially for the lower part of the second horizon in column BP03-19, there are grounds for believing that some maxima were a few years apart.

In the Yudovich [17] diagram of hydrolysate module $(Al_2O_3 + TiO_2 + Fe_2O_3 + FeO + MnO)/SiO_2$ (HM) versus total alkalinity $(Na_2O + K_2O)$ (TA), the sediments of both the horizons of column BP03-19 show identical HM values (from 0.25 to 0.50) corresponding mainly to normal hydrolysate and, in part, low hydrolysate siallites (i.e., silt–clay sediments and clayey silts), and the sediments of column BP03-07 show HM values from 0.2 to 0.3 corresponding to miosilites (in our case, clayey–detrital rocks enriched in quartz). The sediments are even more clearly distinguished by TA values, which increase from the second horizon of column BP03-19, through column BP03-07, to the first horizon

Table 5. Correlation matrix for column BP03-07 (n = 39)

Component	Na_2O	MgO	Al_2O_3	SiO_2	P_2O_5	K_2O	CaO	TiO_2	Cr_2O_3	MnO	FeO	S	V	Ni	Rb
Na_2O	1.00	0.21	0.46	–0.26	–0.09	0.26	–0.20	0.27	–0.09	–0.19	0.14	–0.01	0.20	0.04	0.01
MgO	0.21	1.00	0.80	–0.79	0.18	0.61	–0.23	0.70	0.05	0.30	0.86	–0.18	0.80	0.53	–0.63
Al_2O_3	0.46	0.80	1.00	–0.76	0.10	0.64	–0.22	0.63	0.02	0.01	0.66	–0.18	0.64	0.46	–0.27
SiO_2	–0.26	–0.79	–0.76	1.00	–0.19	–0.63	0.08	–0.48	0.11	–0.35	–0.80	0.14	–0.57	–0.20	0.26
P_2O_5	–0.09	0.18	0.10	–0.19	1.00	0.12	0.02	0.30	–0.13	0.33	0.27	–0.01	0.12	–0.07	0.08
K_2O	0.26	0.61	0.64	–0.63	0.12	1.00	–0.16	0.33	0.08	0.01	0.67	–0.56	0.68	0.42	–0.26
CaO	–0.20	–0.23	–0.22	0.08	0.02	–0.16	1.00	–0.09	–0.09	0.15	–0.19	0.30	–0.33	–0.29	0.19
TiO_2	0.27	0.70	0.63	–0.48	0.30	0.33	–0.09	1.00	–0.03	0.19	0.46	0.07	0.45	0.35	–0.43
Cr_2O_3	–0.09	0.05	0.02	0.11	–0.13	0.08	–0.09	–0.03	1.00	–0.18	0.00	0.04	0.05	0.17	–0.20
MnO	–0.19	0.30	0.01	–0.35	0.33	0.01	0.15	0.19	–0.18	1.00	0.44	0.21	0.08	–0.10	–0.10
FeO	0.14	0.86	0.66	–0.80	0.27	0.67	–0.19	0.46	0.00	0.44	1.00	–0.35	0.83	0.47	–0.53
S	–0.01	–0.18	–0.18	0.14	–0.01	–0.56	0.30	0.07	0.04	0.21	–0.35	1.00	–0.61	–0.46	0.24
V	0.20	0.80	0.64	–0.57	0.12	0.68	–0.33	0.45	0.05	0.08	0.83	–0.61	1.00	0.72	–0.75
Ni	0.04	0.53	0.46	–0.20	–0.07	0.42	–0.29	0.35	0.17	–0.10	0.47	–0.46	0.72	1.00	–0.66
Rb	0.01	–0.63	–0.27	0.26	0.08	–0.26	0.19	–0.43	–0.20	–0.10	–0.53	0.24	–0.75	–0.66	1.00
Sr	–0.13	–0.31	–0.44	0.55	–0.26	–0.56	0.08	0.01	0.07	–0.25	–0.53	0.23	–0.19	0.09	–0.36
Zr	–0.06	–0.75	–0.43	0.47	0.07	–0.41	0.13	–0.43	–0.19	–0.20	–0.70	0.21	–0.80	–0.63	0.92
Ba	–0.17	–0.63	–0.50	0.44	–0.03	–0.35	0.06	–0.28	0.17	0.01	–0.63	0.28	–0.68	–0.43	0.53

Component	Sr	Zr	Ba	1–0.5	0.5–0.25	0.25–0.1	0.1–0.05	Sand	0.05–0.01	0.01–0.005	Silt	0.005–0.001	<0.001	Clay
Na_2O	–0.13	–0.06	–0.17	0.09	0.01	0.12	–0.21	0.10	0.06	0.04	0.06	0.37	–0.17	0.02
MgO	–0.31	–0.75	–0.63	0.33	0.29	0.18	–0.66	–0.39	0.35	0.30	0.38	0.39	–0.23	–0.02
Al_2O_3	–0.44	–0.43	–0.50	0.16	0.19	0.15	–0.56	–0.38	0.19	0.22	0.25	0.42	–0.18	0.03
SiO_2	0.55	0.47	0.44	–0.30	–0.26	–0.36	0.44	0.11	–0.08	–0.21	–0.20	–0.31	0.27	0.09
P_2O_5	–0.26	0.07	–0.03	0.16	–0.19	0.07	–0.18	–0.09	–0.18	0.03	–0.06	0.22	0.00	0.10
K_2O	–0.56	–0.41	–0.35	0.29	0.37	0.52	–0.34	0.03	0.11	0.28	0.26	0.19	–0.39	–0.26
CaO	0.08	0.13	0.06	–0.24	–0.29	–0.18	–0.14	–0.17	–0.18	–0.33	–0.33	0.03	0.41	0.38
TiO_2	0.01	–0.43	–0.28	0.03	0.05	–0.17	–0.76	–0.54	0.31	–0.02	0.13	0.47	0.17	0.36
Cr_2O_3	0.07	–0.19	0.17	0.07	–0.02	–0.21	0.15	–0.60	0.07	–0.12	–0.06	–0.06	0.11	0.06
MnO	–0.25	–0.20	0.01	0.03	0.04	0.33	–0.18	–0.03	–0.27	0.14	–0.02	–0.16	0.03	–0.05
FeO	–0.53	–0.70	–0.63	0.34	0.35	0.48	–0.44	–0.05	0.22	0.41	0.41	0.24	–0.45	–0.29
S	0.23	0.21	0.28	–0.18	–0.26	–0.48	0.00	–0.36	–0.23	–0.49	–0.48	0.11	0.56	0.54
V	–0.19	–0.80	–0.68	0.30	0.40	0.26	–0.46	0.00	0.54	0.51	0.63	0.29	–0.52	–0.32
Ni	0.09	–0.63	–0.43	0.02	0.21	0.03	–0.29	–0.13	0.54	0.57	0.67	0.04	–0.38	–0.32
Rb	–0.36	0.92	0.53	–0.20	–0.31	0.16	0.43	0.09	–0.75	–0.36	–0.62	–0.22	0.26	0.13
Sr	1.00	–0.10	0.19	–0.28	–0.14	–0.72	–0.05	–0.13	0.50	–0.10	0.15	–0.04	0.33	0.27
Zr	–0.10	1.00	0.61	–0.25	–0.33	–0.01	0.46	0.11	–0.68	–0.40	–0.61	–0.27	0.36	0.19
Ba	0.19	0.61	1.00	–0.26	–0.29	–0.18	0.40	0.07	–0.40	–0.29	–0.40	–0.36	0.37	0.16

of column BP03-19 (Fig. 8). This trend is interpreted here as reflecting a facies transition from marginal filter conditions to marine–fluvial and further to marine sedimentation environments (with a seaward increase in the mobility of alkalis, especially Na, during geochemical differentiation). The established chemical features can be clearly illustrated by comparing the average compositions of the two horizons of column BP03-19 and column BP03-07 sediments (Table 6). In particular, it is clearly seen that the column BP03-07 sediments are

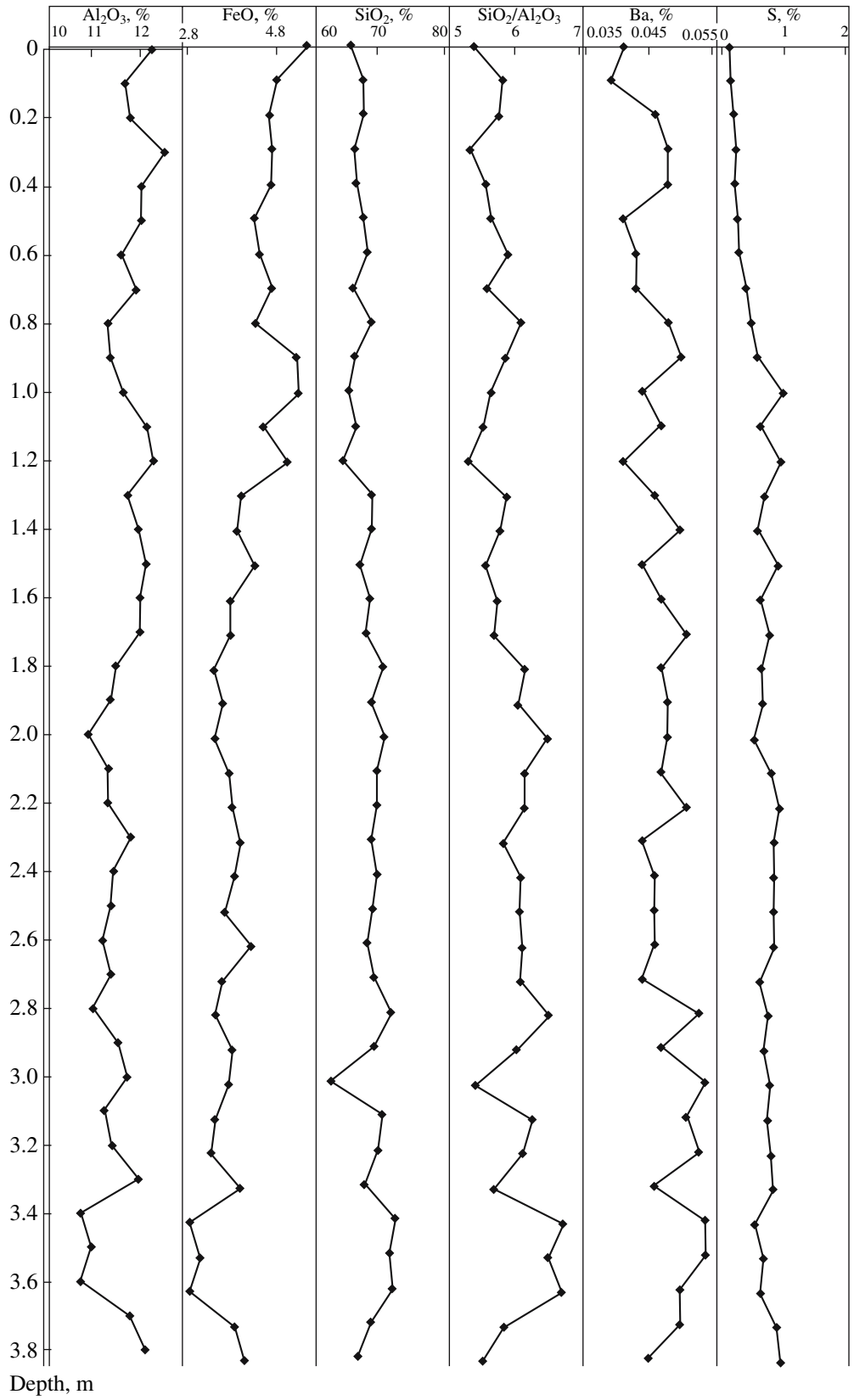

Fig. 6. Chemical composition of sediments from column BP03-07.

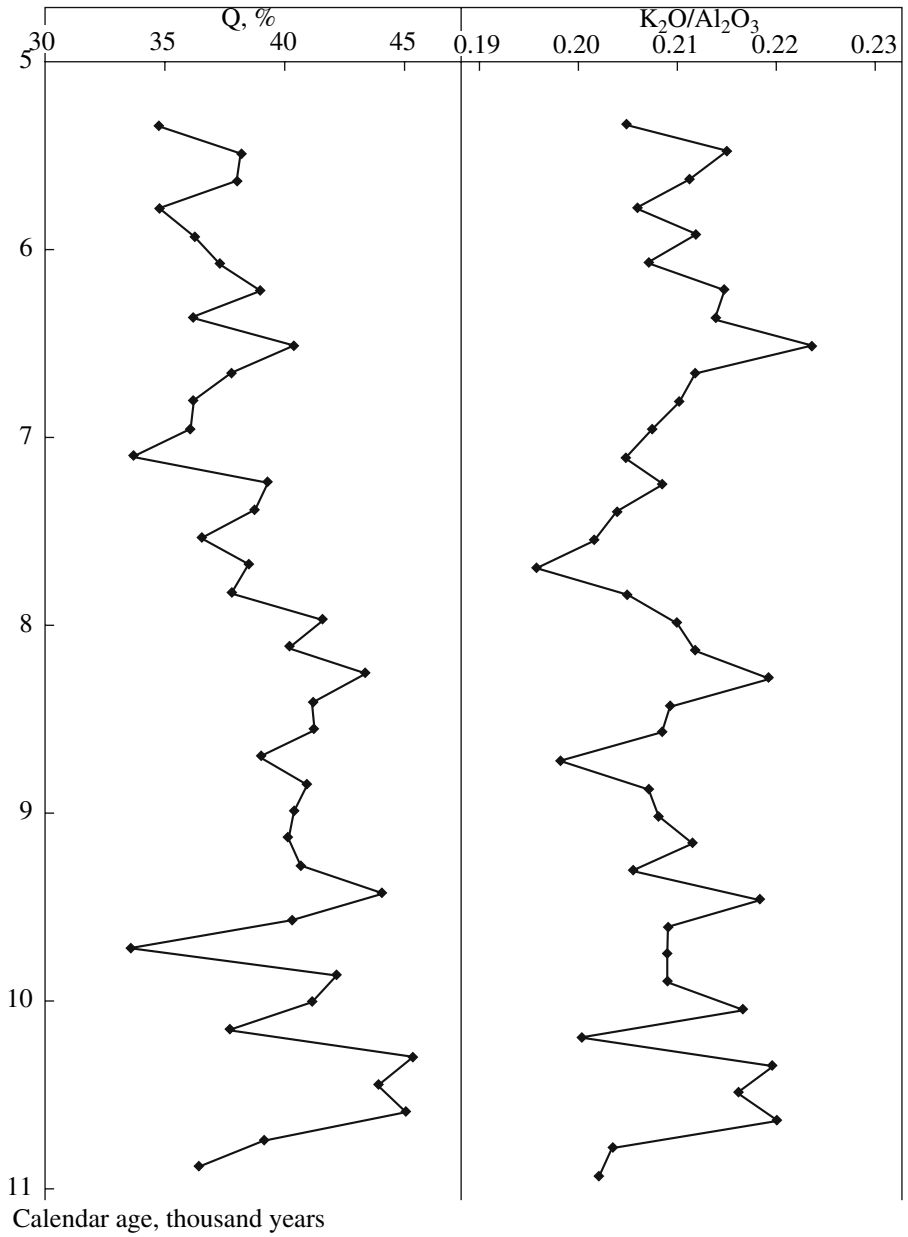

Fig. 7. Distribution of indicator parameters of the sediment discharge of the Ob River, quartz content (Q) and K_2O/Al_2O_3 ratio, against the age of sediments in column BP03-07.

enriched relative to the more southern column in SiO_2, Ni, Sr, and Ba but depleted in MnO, FeO, MgO, Al_2O_3, P_2O_5, LOI, Rb, TiO_2, and Cr_2O_3.

Column DM-4397

This column was recovered not far to the north of column BP03-07 (Fig. 1) on the slope of the Ob–Yenisei shoal. The lithology of the column was described by Levitan et al. [14], and the data on benthic foraminifera, mineral composition, oxygen and carbon isotopes in the shells of secretion foraminifera, and two radiocarbon datings were presented in [18]. Demina et al. [19] reported the distribution of bulk concentrations and speciation of Fe, Mn, Zn, Cu, Co, Cr, Ni, and Pb in the column.

Two main lithostratigraphic horizons, 0–190 and 190–384 cm, can be distinguished from top to bottom. The upper horizon is composed of olive gray (except for the oxidized upper brown layer) marine silty–pelitic (0–70 cm) and pelitic (70–190 cm) muds with characteristic bioturbation structures and hydrotroilite streaks. The lower horizon is made up of greenish gray silty–pelitic muds with interbeds of black silts and silty sands in the middle part (250–280 cm) and pebble-

bearing massive sands at the base of the section. A bivalve shell was found at a depth of 275 cm.

The total number of benthic carbonate foraminifers increases downward from 0 to 40 per gram of sediment, then decreases abruptly at a depth of 235 cm to 10 individuals per gram, increases again to 40 at 260 cm, and declines to zero at the base of the column. The number of marine forms proper (*C. reniforme*) increases upward from the bottom of the section to the 240 cm level, whereas the number of forms residing in the zone of mixing of river and sea waters (*E. clavatum*) decreases toward the 190 cm level. The oxygen of *E. clavatum* shells is enriched in ^{16}O downward, especially starting from a depth of 210 cm, whereas the carbon isotopic composition becomes heavier in the same direction, especially below 230 cm. The content of clinopyroxene increases significantly downward from 230 cm. In general, the sediments of the section show a downward increase in the bulk content of Fe, Zn, Cu, Co, Cr, and, to some extent, Pb starting on average from 190 cm.

The calendar age of the samples of mixed foraminifer complexes is 8150 yr at a level of 190 cm and 9805 yr at 280 cm. Thus, the calendar age of the boundary between the marine horizon and the horizon showing significant river influence is 8.15 kyr; the sedimentation rate is 23.3 cm/kyr in the upper horizon (assuming that the section terminated by modern sediments was not disturbed) and 54.4 cm/kyr in the lower horizon. The

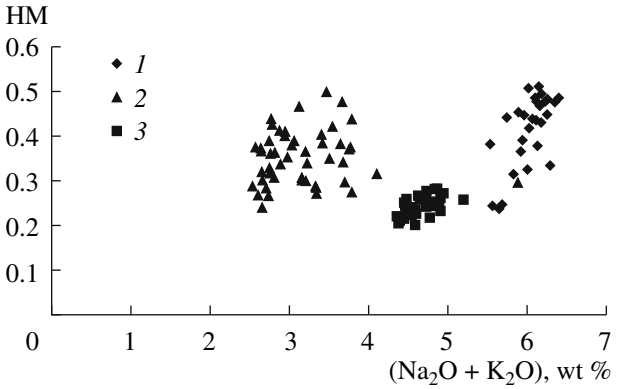

Fig. 8. Module diagram HM—$Na_2O + K_2O$ (see text for explanation). (*1*) Sediments of the first horizon of column BP03-19, (*2*) sediments of the second horizon of column BP03-19, and (*3*) sediments of column BP03-07.

Table 6. Chemical compositions of sediments from the columns of the Ob transect

Column no.		Na_2O, %	MgO, %	Al_2O_3, %	SiO_2, %	P_2O_5, %	K_2O, %	CaO, %
BP03-07 (n = 39)		2.08–2.57 / 2.21	1.28–2.00 / 1.71	10.78–12.58 / 11.68	63.63–72.9 / 68.94	0.06–0.093 / 0.077	2.35–2.59 / 2.44	0.95–1.96 / 1.22
BP03-19	0–1.52 m (n = 30)	3.11–4.12 / 3.57	1.89–3.05 / 2.53	11.58–14.22 / 13.42	49.14–61.21 / 54.27	0.113–0.348 / 0.258	2.27–2.63 / 2.50	0.81–1.38 / 0.94
	1.52–6.7 m (n = 52)	0.42–3.48 / 1.07	1.47–2.64 / 2.13	10.82–14.84 / 12.88	51.77–69.53 / 60.60	0.055–0.285 / 0.153	2.08–2.41 / 2.23	0.99–2.47 / 1.26
Column no.		TiO_2, %	Cr_2O_3, %	MnO, %	FeO, %	LOI	S, %	V, %
BP03-07 (n = 39)		0.646–0.773 / 0.728	0.01–0.023 / 0.013	0.047–0.27 / 0.073	2.87–5.48 / 4.05	3.68–7.46 / 5.58	0.12–0.98 / 0.64	0.0098–0.0172 / 0.0132
BP03-19	0–1.52 m (n = 30)	0.71–0.81 / 0.77	0.018–0.024 / 0.022	0.096–0.594 / 0.263	6.7–10.64 / 9.12	9.05–14.24 / 11.86	0.19–2.29 / 0.38	0.0137–0.0184 / 0.0167
	1.52–6.7 m (n = 52)	0.65–0.94 / 0.80	0.014–0.036 / 0.019	0.053–0.433 / 0.145	4.15–9.98 / 6.73	5.52–15.82 / 11.36	0.16–2.78 / 0.70	0.0091–0.0161 / 0.0121

Column no.		Ni, %	Rb, %	Sr, %	Zr, %	Ba, %
BP03-07 (n = 39)		0.0051–0.0083 / 0.0065	0.0038–0.0103 / 0.0058	0.026–0.040 / 0.032	0.015–0.030 / 0.020	0.039–0.054 / 0.047
BP03-19	0–1.52 m (n = 30)	0.0041–0.0066 / 0.0053	0.0063–0.0088 / 0.0080	0.010–0.023 / 0.013	0.009–0.021 / 0.012	0.038–0.049 / 0.044
	1.52–6.7 m (n = 52)	0.0032–0.0061 / 0.0046	0.0073–0.0104 / 0.0090	0.008–0.036 / 0.020	0.014–0.030 / 0.020	0.024–0.052 / 0.038

Note: Maximum and minimum values are shown in the numerator, and arithmetic mean is given in the denominator.

lower 4 cm of the column are probably composed of purely riverine sediments (this is suggested by their lithology and the complete absence of foraminifers) belonging to seismostratigraphic unit II [20]. Then, the age of their roof is approximately 11.6 calendar kyr, which approximately corresponds to the base of the Holocene (similar to the two above-described columns). Thus, river influence decreases regularly from bottom to top in the section, approximately to the level of 8.15 calendar kyr. The sediment discharge of the Ob increased definitely only within the interval 9.25–9.80 calendar kyr. It is noteworthy that this interval is in good agreement with the above-described data for column BP03-07 and the sediment discharge of the Yenisei. On average, the sedimentation rate of the river horizons of all the columns decreases northward.

DISCUSSION

We can now make some unequivocal conclusions as to the history of the sediment discharge of the Ob. First, the columns described here probably represent sediments from a single channel of the Proto-Ob, which originated at the Pleistocene–Holocene boundary. This suggestion is in agreement with the data on column BP00-38, which was recovered north of the zone of mixing of Ob and sea waters and for which three radiocarbon age determinations were published [20]. Second, the geochemistry of early Holocene deposits provides compelling evidence that the sediments of the zone of mixing of river and sea waters are replaced from south to north along the Ob transect by marine–fluvial and fluvial–marine facies. Third, it should be noted that marine–fluvial sedimentation ceased in the channel of this river at the middle Holocene. Taking into account that similar processes in the northern part of the Ob–Yenisei shoal were related to the channels of the Proto-Yenisei (columns BP00-36/4 and BP01-39/2 [10]), it can be supposed that the middle Holocene glacioisostatic upwelling of the crustal segments that were covered in the late Valdai by the Kara ice sheet [10] affected also the adjoining regions of the Ob–Yenisei shoal. Fourth, there is a fairly clearly defined trend of a decrease in river influence during the early Holocene, probably markedly disturbed during the stage of 9.80–9.25 ka. Fifth, there are grounds to suggest that the Ob and Yenisei underwent similar histories of river discharge in the Holocene. This is understandable, because their catchments occur in very similar climatic conditions.

Noteworthy are the results of Kremenetski et al. [21] on the timing of the beginning of peat bog formation in western Siberia. These authors invoked considerable statistical data on the radiocarbon dating of peats and correlated the main peak in the intensity of their formation with the period from 11 to 7 calendar kyr (with a maximum at 10 kyr). It should be noted also that this age interval is close to the period of the maximum (judging from sedimentation rates) sediment discharge of the Yenisei and the elevated discharge of river material in the channel of the Proto-Ob. This similarity could be related to the elevated humidity caused primarily by intense thawing in the permafrost areas of the catchments [21].

There are probably grounds to believe that the diagenetic processes of ikaite crystallization, which were described in detail by Kodina et al. [15, 16], were confined to sediments formed in a certain facies environment strongly influenced by river discharges in paleochannels during the first half of the Holocene.

ACKNOWLEDGMENTS

This study was financially supported by the Russian Foundation for Basic Research, project nos. 02-05-64017 and 05-05-64342; the Federal Program "World Ocean," project no. 43.634.11; and Program no. 34P of the Presidium of the Russian Academy of Sciences.

REFERENCES

1. L. P. Bobylev, K. Ya. Kondratyev, and O. M. Johannessen, *Arctic Environment Variability in the Context of Global Change* (Springer, Berlin, 2003).
2. R. Stein, "Arctic Paleo-River Discharge (APARD)," Ber. Polarforsch., No. 279 (1998).
3. V. V. Gordeev, J. M. Martin, I. S. Sidorov, and M. V. Sidorova, "A Reassessment of the Eurasian River Input of Water, Sediment, Major Elements, and Nutrients to the Arctic Ocean," Am. J. Sci. **296**, 664–691 (1996).
4. M. A. Levitan, M. V. Burtman, L. L. Demina, et al., "History of Holocene Sedimentation in the Southern Kara Sea," Litol. Polezn. Iskop, No. 6, 651–666 (2004) [Lithol. Min. Res. **39**, 566–579 (2004)].
5. M. A. Levitan, M. V. Burtman, L. L. Demina, et al., "Facies Variability of Surface Sediments from the Ob–Yenisei Shoal and the Ob and Yenisei Estuaries," Litol. Polezn. Iskop, No. 5, 472–484 (2005) [Lithol. Min. Res. **39**, 408–419 (2005)].
6. K. Dittmers and F. Schoster, "Acoustic Facies in the Southern Kara Sea: New Results by PARASOUND Echosounding," Ber. Polarforsch., No. 479, 55–71 (2004).
7. M. A. Levitan, V. V. Krupskaya, E. A. Frolova, and L. N. Vlasova, "First Results of the Sediment Studies," Ber. Polarforsch., No. 479, 44–54 (2004).
8. F. Schoster and M. A. Levitan, "Scientific Cruise Report of the Kara Sea Expedition with RV "Akademik Boris Petrov" in 2003 within the Frames of the Russian–German Project 'SIRRO' and the Russian–Norwegian Project 'MAREAS'," Ber. Polarforsch., No. 479 (2004).
9. V. P. Petelin, *Grain-Size Analysis of Marine Bottom Sediments* (Nauka, Moscow, 1967) [in Russian].
10. R. Stein, F. Niessen, K. Dittmers, et al., "Siberian River Run-Off and Late Quaternary Glaciation in the Southern Kara Sea, Arctic Ocean: Preliminary Results," Polar Res. **21**, 315–322 (2002).
11. M. Stuiver, P. J. Reimer, E. Bard, et al., "INTCAL 98 Radiocarbon Age Calibration, 24.000–0 Cal BP," Radiocarbon **40**, 1041–1083 (1998).

12. M. A. Levitan, M. V. Burtman, Z. N. Gorbunova, and E. G. Gurvich, "Quartz and Feldspars in the Surface Layer of Kara Sea Sediments," Litol. Polezn. Iskop, No. 2, 115–125 (1998) [Lithol. Min. Res. **33**, 99–108 (1998)].
13. F. Schoster and R. Stein, "Major and Minor Elements in Surface Sediments of Ob and Yenisei Estuaries and the Adjacent Kara Sea," Ber. Polarforsch., No. 300, 196–207 (1999).
14. M. A. Levitan, T. A. Khusid, V. M. Kuptsov, et al., "Type Sections of the Upper Quaternary Deposits of the Kara Sea," Okeanologiya, No. 5, 776–788 (1994).
15. L. A. Kodina, V. G. Tokarev, L. N. Vlasova, and G. S. Korobeinik, "Contribution of Biogenic Methane to Ikaite Formation in the Kara Sea: Evidence from the Stable Carbon Isotope Geochemistry," in *Siberian River Run-Off in the Kara Sea. Characterisation, Quantification, Variability and Environmental Significance*, Ed. by R. Stein, K. Fahl, D. Futterer, et al. (Elsevier, Amsterdam, 2003), pp. 349–374.
16. I. Mardanian and L. Kodina, "Organic Carbon Distribution within Two Ikaite-Bearing Sediment Cores in the Kara Sea," Ber. Polarforsch., No. 479, 72–76 (2004).
17. Ya. E. Yudovich and M. P. Ketris, *Principles of Lithochemistry* (Nauka, St. Petersburg, 2000) [in Russian].
18. L. Polyak, M. Levitan, T. Khusid, et al., "Variations in the Influence of Riverine Discharge on the Kara Sea during the Last Deglaciation and the Holocene," Global Planet. Change **32**, 291–309 (2002).
19. L. L. Demina, M. A. Levitan, and N. V. Politova, "Speciation of Metals in the Sediments of the Kara Sea," Geokhimiya, (in press).
20. K. Dittmers, F. Niessen, and R. Stein, "Holocene Sediment Budget and Sedimentary History of the Ob and Yenisei Estuaries, in *Siberian River Run-Off in the Kara Sea. Characterisation, Quantification, Variability and Environmental Significance*, Ed. by R. Stein, K. Fahl, D. Futterer, et al. (Elsevier, Amsterdam, 2003), pp. 457–488.
21. K. V. Kremenetski, A. A. Velichko, O. K. Borisova, et al., "Peatlands of the Western Siberian Lowlands: Current Knowledge on Zonation, Carbon Content and Late Quaternary History," Quatern. Sci. Rev. **22**, 703–723 (2003).